Microtubule reorganization during mitotic cell division in the dinoflagellate *Ostreospis* cf. *ovata*

David Velasquez-Carvajal[1,3], Flavie Garampon[1], Rodolphe Lemée[2], Sebastian Schaub[1] and Stefania Castagnetti[1*]

[1] Sorbonne Universités, CNRS, Laboratoire de Biologie du Développement de Villefranche-sur-Mer (LBDV), 06230 Villefranche-sur-Mer, France.

[2] Sorbonne Université, CNRS, Laboratoire d'Océanographie de Villefranche, LOV, F-06230, Villefranche-sur-Mer, France

[3] current address: Grupo de investigación en neurociencias y envejecimiento. Facultad de Ciencias de la Salud. Corporación Universitaria Remington. calle 51 n.° 51-27, Medellín, Colombia.

* corresponding author: stefania.castagnetti@imev-mer.fr

Running title: Microtubules in dinomitosis

Keywords: dinoflagellates, microtubules, mitosis, cytokinesis, centrin

Summary statement

Our study describes special features of mitosis and cytokinesis in dinoflagellates and uncovers a new alternative mechanism for cell division, highlighting the plasticity of cell biological process in eukaryotic cells.

Abstract

Dinoflagellates are marine organisms that undergo seasonal explosive proliferation events known as algal blooms. Vegetative cell proliferation is a main contributing factor in these events. However, mechanistical understanding of mitosis and cytokinesis in dinoflagellate remains rudimentary. Using an optimized immunofluorescence protocol, we analysed changes in microtubule organization occurring during the mitotic cycle of the toxic dinoflagellate *Ostreopsis* cf. *ovata.* This study revealed important features of dinoflagellate cell division. We find that the two flagella and the cortical microtubule array persist throughout the mitotic cycle. Two microtubule bundles are present in the cytoplasm originating from the ventral area, where the basal bodies are located: a cortical bundle and a cytoplasmic ventral bundle. The latter associates with the nucleus in the cell centre in preparation for mitosis and with the acentrosomal extranuclear spindle during mitosis. Analysis of tubulin post-translational modifications identifies two populations of spindle microtubules: polar acetylated microtubules whose length is stable throughout mitosis and central tyrosinated microtubules which elongate during chromosome segregation. During cell division a microtubule rich structure forms along the dorsal-ventral axis, associated with the site of cytokinesis, consistent with a cytokinetic mechanism independent of the actomyosin ring typical of animal and yeast cells.

Introduction

Dinoflagellates are unicellular eukaryotes that have adapted to most aquatic ecosystems, from tropical to polar waters. These protists are known to undergo large population expansions that can impact heavily on the marine ecosystem and on human health, a phenomenon known as Harmful Algae Bloom (HAB) (Driscoll et al., 2016). Despite the extensive investigations into the ecological and cellular basis of HABs, the mechanisms controlling dinoflagellate cell proliferation, a major process underlying HAB development, still remain elusive.

Dinoflagellate mitosis, also known as dinomitosis, is unique among eukaryotes. It is a form of closed mitosis, where chromosome segregation occurs within the nucleus, without nuclear envelope breakdown. Differently from yeasts, diatoms and euglenoids, which undergo closed mitosis with a nuclear spindle, in dinoflagellates spindle microtubules are cytoplasmic and traverse the nucleus through tunnels never entering the nucleoplasm (Gavelis et al., 2019). Segregating chromosomes are attached to the nuclear membrane surrounding the nuclear tunnels, through electron dense kinetochore-like structures, which in turn contact microtubules on the cytoplasmic side (Cachon and Cachon, 1977; Oakley and Dodge, 1974). Hence, the interaction between spindle microtubules and segregating chromosomes is indirect, across the nuclear membrane. This configuration poses the question of how the spindle is organized in these organisms and how chromosomes are segregated within the nuclear membrane. EM studies in *Syndinium* (Ris and Kubai, 1974) and in *Amphidinium carterae* (Oakley and Dodge, 1976) showed that the microtubules emanating from the kinetochore-like structures extend exclusively towards the nearby polar region of the spindle and the kinetochore to pole distance remains constant throughout mitosis. Thus, chromosome segregation was suggested to be accomplished by elongation of cytoplasmic microtubules running through the nuclear channels between the two spindle poles

Following nuclear division, the cell divides during cytokinesis. In animal and yeast cells, cytokinesis relies on the constriction of an actomyosin ring. The absence of identifiable myosin-II in many bikonts (Richards and Cavalier-Smith, 2005), including dinoflagellates,

however, suggests that an alternative mechanism for cytokinesis must be in place in these organisms. In plants a transient ring of cortical microtubules and actin filaments, the preprophase band, forms early in the cell cycle and marks the site of cytokinesis. During anaphase an equatorial array of microtubules, the phragmoplast, then directs Golgi-derived vesicles to the cortical division site to allow deposition of the new cell wall (Nishihama and Machida, 2001). Mechanisms of cytokinesis that do not involve an actomyosin ring have also been described for many single-celled protists. In *Trypanosoma brucei* cell division occurs by microtubule dependent formation of a unidirectional furrow from the anterior to the posterior of the cell (Sherwin et al., 1989). In *Chlamydomonas reinhardtii* and many related green algae, a microtubule structure, called the phycoplast, forms between the duplicated basal bodies at the anterior of the cell and then grows towards the posterior pole (Ehler and Dutcher, 1998). Actin also accumulates at this site, but treatment with actin depolymerizing drugs does not induce any defect in cell division (Onishi et al., 2020). For dinoflagellates, little is known on how cytokinesis takes place and the contribution of the cytoskeleton to this process. Early EM studies in *A. carterae* (Oakley and Dodge, 1976) and in *Ceratium tripos* (Wetherbee, 1975) showed that cell division occurs by pinching in of the membrane in the equatorial region where microtubules accumulate under the plasma-membrane. Treatment with actin depolymerizing drugs, however, was shown to interfere with completion of cell division in *Prorocentrum micans*, suggesting a contribution of the actin cytoskeleton to cytokinesis, at least in some species (Schnepf et al., 1990).

To gain further insights into the mechanism of dinomitosis and the organization of the mitotic spindle in dinoflagellates, we analysed the spatial and temporal changes in cytoskeletal organization during the mitotic cycle in the dinoflagellate *Ostreopsis* cf. *ovata* (*O.* cf. *ovata*), one of the most common HAB causing species in tropical and subtropical areas (Parsons et al., 2012; Rhodes, 2011) and the most abundant and widely distributed benthic dinoflagellate in the Mediterranean Sea (Ninčević Gladan et al., 2019). *O.* cf. *ovata* cells have a teardrop shape with a pointy ventral side, from which two flagella emanate and a rounded dorsal side, where the nucleus is located during interphase. In interphase cells, a cortical array of microtubules underlies the plasma membrane (cortical microtubule

105 array) and a microtubule bundle runs from the ventral sulcal area towards the inside of the
106 cell (Escalera et al., 2014). Here we show that the cortical microtubule array and the flagella
107 persist throughout the cell cycle. We also analyse changes in the organization of
108 microtubule-based structures during the mitotic cycle and describe novel ultrastructural
109 features of the microtubule cytoskeleton as cells undergo mitosis and cytokinesis. We find
110 that microtubules of the ventral bundle contact the nucleus while it localizes to the centre
111 of the cell in preparation for mitosis. An acentrosomal microtubule-based spindle then
112 forms in the cell centre, transverses the nucleus and separates chromosomes. Analysis of
113 tubulin posttranslational modifications identifies two regions in the anaphase spindle: a
114 stable polar spindle enriched in acetylated tubulin, linking chromosomes to the ventral
115 bundle and a dynamic central spindle, containing tyrosinated tubulin, between separating
116 chromosome masses. In dividing cells, a microtubule-rich structure, free of actin, forms
117 from the dorsal side along the longitudinal axis of the cell where cytokinesis takes place,
118 and divides the cell. Our observations reveal that both mitosis and cytokinesis in *O.* cf.
119 *ovata* are different from yeast and animal cells and support the idea that the mechanisms
120 of cell division are highly diverse outside of opisthokonts.

121

122 **Results**

123 **Cortical microtubule array and flagella are maintained throughout the cell cycle**

124 To analyse the changes in the organization of the microtubule cytoskeleton associated with
125 the mitotic cell cycle in *O.* cf. *ovata* we have optimized an immunofluorescence protocol
126 previously developed to stain cortical microtubules (Escalera et al., 2014). We applied it
127 to label microtubules in both cultured cells and wild samples collected in the Bay of
128 Villefranche-sur-mer during summer blooming and obtained similar results with both
129 sources of cells. Staining using the ß-tubulin D66 antibody labelled several structures in
130 the cell (Fig. 1A). Previous description of microtubules in *O.* cf. *ovata* had identified a
131 network of microtubules underlying the plasma membrane in interphase cells (Escalera et
132 al., 2014). We confirmed the presence of this cortical microtubule array (Fig. 1A and movie
133 1). On the posterior side of the cell, cortical microtubules ran vertically along the dorso-

134 ventral axis covering the entire surface of the cell. On the opposite anterior side, recognized
135 by the presence of the apical pore, instead, cortical microtubules run obliquely from the
136 apical pore to the side of the cell. The anterior and posterior halves are separated by the
137 cingulum, which circles the entire cell (Fig. 1A). The cingulum is delimited by two parallel
138 bands of microtubules, while in the groove of the cingulum tightly packed parallel
139 microtubules run transversally, perpendicular to the lateral bands (Fig. 1A, lateral view).
140 Two previously identified thick bundles of MTs originating from microtubular roots
141 present in the ventral sulcal area, can also be observed: one close to the cell surface on the
142 posterior side of the cell, which we named cortical bundle (CB), and a second deeper in the
143 cytoplasm, herein referred to as ventral bundle (VB, Fig. 1A and movie 1). Specificity of
144 the observed tubulin staining was confirmed by treatment of cells with the microtubule
145 depolymerizing drug colchicine for 1 hour prior to fixation. All microtubules were lost in
146 colchicine treated samples but not in control (dH2O) samples (Fig. 1B).

147 Using bloom samples collected between 12pm and 4am, which as previously showed are
148 enriched in mitotic and dividing cells (Pavaux et al., 2021), we then asked whether cortical
149 microtubules were maintained throughout the cell cycle. In *O.* cf. *ovata* different cell cycle
150 stages can be identified based on morphological features and on the characteristic position
151 of the nucleus within the cell (Bravo et al., 2012; Pavaux et al., 2021). The nucleus which
152 is located in the dorsal area during interphase (non-dividing cells) relocates to the cell
153 centre in preparation for mitosis (pre-mitotic cells), where the nucleus divides (mitotic
154 cells). Following mitosis binucleated cells divide (cytokinesis) by fission and, using
155 brightfield microscopy a furrow can be observed bisecting the cell to give rise to two post-
156 dividing cells recognized by the presence of the nucleus in lateral position.

157 We observed that the cortical array of microtubules is stable and persists throughout the
158 cell cycle: in interphase, pre-mitotic, mitotic and post-dividing cells (Fig. 1C). Similarly,
159 flagella, emanating from the ventral pole, were present at all stages of the cell cycle,
160 including mitosis and cytokinesis (Fig. S1). This is in contrast with what was previously
161 described in another dinoflagellate species *Crypthecodinium cohnii* (Perret et al., 1993) or

162 in other algal species like *C. reinhardtii*, where flagella are absent during mitotic cell
163 division (Cross and Umen, 2015; Rosenbaum et al., 1969).

164 **Changes in microtubule organization during mitosis and cytokinesis**

165 In most interphase cells (> 95%), the two microtubule bundles (VB and CB) extend for a
166 third to half of the cell length towards the cell centre (Fig. 2A, interphase). The cortical
167 bundle is a stable thick bundle of microtubules most likely associated with the flagellar
168 apparatus to anchor the basal bodies to the cell cortex, comparable to the rootlet
169 microtubule of *C. reinhardtii* (Rosenbaum et al., 1969). The ventral bundle instead is a
170 more dynamic structure which changes during the cell cycle. During interphase,
171 microtubules of the VB are compacted for most of the length of the bundle but thin
172 ramifications can be observed extending in the cell centre (Fig. 2A, interphase). In few
173 interphase cells (< 5%), the ventral bundle extends past the cell mid-line and reaches the
174 nucleus in dorsal position (Fig. 2A, interphase). In pre-mitotic cells, when the nucleus is
175 positioned in the cell centre, microtubules branching from the ventral bundle contact the
176 nucleus, forming a structure that resembles an inverted "Y" (Fig. 2A and Fig. S2, pre-
177 mitotic) and enveloping the ventral side of the nucleus.

178 In mitotic cells, microtubules then organize in 6 to 8 parallel bundles (n= 5 cells) that align
179 along the short axis of the cell to form the mitotic spindle (Fig. 2A and Fig. S2,
180 pro/metaphase), suggesting the presence of 6-8 nuclear tunnels. Spindle microtubules
181 converge at two opposite poles which are connected to the ventral area of the cell by thin
182 microtubule bundles (Fig. 2A), probably originating from splitting of the ventral bundle
183 present in interphase cells. No astral microtubules are visible in mitotic cells. As previously
184 reported for other dinoflagellate species (Bhaud et al., 2000), we observed that in early
185 mitosis, the DNA concentrates in the central region of the spindle onto a metaphase-like
186 plate (Fig. 2A, pro/metaphase), before separating into two discrete masses during anaphase
187 (Fig. 2A and Fig. S2, anaphase). Measurement of pole to pole distance showed that spindle
188 length is constant prior to chromosome segregation (pro/metaphase; average ± SD: 12,1 ±
189 1,3 µm) and spindle elongation is observed only following chromosome segregation in
190 anaphase when spindle length extends up to 27,5 µm (Fig. 2B). However, we observed that

191 pole to DNA distance, measured as distance between the middle of each DNA mass and
192 the corresponding spindle pole, remains constant during mitosis from prophase to telophase
193 (Fig. 2C; average ± SD: pro/metaphase: 5,95 ± 0,6 µm; anaphase: 5,7± 0,6 µm; telophase:
194 6,1± 0,5 µm). Thus, chromosome segregation appears to be driven exclusively by extension
195 of the central spindle region.

196 As shown in Fig. 2A (anaphase, arrowhead), in many anaphase cells, microtubules also
197 accumulate in the dorsal area of the cell. By analysing cells at different mitotic stages, we
198 noticed that a dorsal enrichment in microtubules could be observed already at earlier
199 mitotic stages. This microtubule-rich structure corresponds to the site of cytokinesis (Fig.
200 2A and Fig. S2, telophase/cytokinesis and Fig. 3A). Three-D reconstruction of cells at
201 different stages of mitosis showed that this microtubule structure develops progressively.
202 In early mitotic cells, up to anaphase, microtubules first arrange in a ring, perpendicular to
203 the cingulum, under the cell surface (Fig. 3A, metaphase/anaphase). As cells progress
204 through anaphase microtubules fill the space between the dividing cells (Fig. 3A,
205 telophase) and by the end of mitosis, when chromosomes are fully segregated to opposite
206 sides of the cell and the central spindle is no longer visible, microtubules fill the entire
207 surface between the two daughter cells, forming a dense microtubule plate (Fig. 3A,
208 cytokinesis).

209 The presence of a microtubule rich plate at the site of cell division suggests that cytokinesis
210 is driven by microtubules in *O.* cf. *ovata*. This is consistent with observations in other
211 protists where microtubule-rich structures drive cell division and are essential for
212 cytokinesis (Ehler and Dutcher, 1998; Francia et al., 2015; Hammarton, 2019; Onishi et
213 al., 2020; Sherwin et al., 1989). Although microtubule enrichment at the cleavage furrow
214 was already observed in dinoflagellates, actin is thought to be required for completion of
215 cell division in some dinoflagellates species, like *P. micans* (Schnepf et al., 1990). We
216 therefore asked whether actin microfilaments are enriched at the cytokinetic plate. Similar
217 to what was previously observed in other dinoflagellate species (Schnepf, 1988; Villanueva
218 et al., 2014), staining with phalloidin showed a diffuse cytoplasmic grid-like pattern (Fig.
219 3B) which was lost following 5 minutes of treatment with the actin depolymerizing drug

220 latrunculin-A (10 µM, Fig. 3C). Interestingly latranculin A treated cells quickly lost their
221 shape and often become round within 5 minutes of treatment. In untreated cells, we
222 observed actin fibres connecting the cell cortex to the cell centre, where the phalloidin
223 staining is more concentrated. In all cells, irrespectively of cell cycle stage, actin also
224 accumulated around the nucleus (Fig. 3B), as previously described in *C. cohnii* (Perret et
225 al., 1993) and *L. polyedra* (Schnepf, 1988; Stires and Latz, 2018). No discrete actin-
226 containing structure was observed at the site of division, further supporting the existence
227 of a microtubule-based mechanism both for chromosome segregation and for cytokinesis
228 in *O.* cf. *ovata*.

229

230 **Different microtubular sub-populations drive cell division**

231 All microtubules are formed by α/ß-tubulin heterodimers whose properties are modulated
232 by post-translational modifications (PTMs) (Bulinski et al., 1988; Janke, 2013; Wolff et
233 al., 1992). Among all identified PTMs, acetylation, tyrosination and poly-glutamylation
234 (Fig. 4A) appear to be conserved across most eukaryotes. We reasoned that analysing
235 tubulin PTMs would allow to distinguish between different sub-populations of
236 microtubules and their changes during the cell cycle, providing insight into how the
237 cytoskeletal structures described above are generated and are related to one another. We
238 therefore analysed tubulin tyrosination, acetylation and poly-glutamylation during *O.* cf.
239 *ovata* cell division (dinomitosis and cytokinesis). We first tested whether these tubulin
240 PTMs could be detected in *O.* cf. *ovata* protein extracts by western blot using specific
241 antibodies. We used the YL1/2 monoclonal antibody which recognizes the C-terminal EEF
242 sequence of yeast α-tubulin (Kilmartin et al., 1982), conserved in *O.* cf. *ovata* α-tubulin; a
243 monoclonal antibody (T6793) which specifically recognizes acetylated lys40 of α-tubulin,
244 and the antibody GT335 against mouse poly-glutamylated tubulin (Wolff et al., 1992). As
245 shown in Fig. 4B, YL1/2 and T6793 antibodies recognized a single protein of the same
246 size as α-tubulin.

247 Tyrosinated α-tubulin corresponds usually to newly polymerized and dynamic
248 microtubules, whereas removal of the carboxy-terminal tyrosine residue (detyrosination)
249 marks microtubule aging and stabilization (Bulinski et al., 1988; Schulze et al., 1987).
250 Immunolabelling of cycling *O.* cf. *ovata* cells using the YL ½ antibody showed that
251 tyrosinated tubulin is present in the flagella, in the cortical array and in the ventral bundle
252 at all cell cycle stages (Fig. 4C, interphase and Fig. S3A). In mitotic cells both in early
253 (pro/metaphase), and late (anaphase) stages, the YL ½ antibody labelled the central region
254 of the spindle near the midplane, but no signal was detected in the polar spindle regions
255 until telophase (Fig. 4C, mitosis).

256 Acetylation of lysine 40 (lys40) on α-tubulin instead was shown to be often associated with
257 stable long-lived microtubules (Eshun-Wilson et al., 2019). Immunostaining with the
258 T6793 antibody showed that, at all cell cycle stages, both the cortical array and flagella
259 contain acetylated microtubules (Fig. S3B). Differently from tyrosinated tubulin, in early
260 mitotic cells, before chromosome segregation (pro/metaphase), tubulin acetylation extends
261 over the entire length of the spindle, including the polar region. However, in anaphase cells,
262 following chromosome segregation, acetylated α-tubulin is restricted to the polar region of
263 the spindle which is associated with the DNA (Fig. 4C), but is absent in the central spindle
264 (between the segregating chromosomes). Acetylated-tubulin was also detected at the site
265 of cytokinesis both in the early-cytokinetic ring and in the late-cytokinetic plate (Fig. 4C).
266 Co-staining of *O.* cf. *ovata* cells for acetylated and tyrosinated tubulin did not allow to
267 identify any difference in the cortical array (Fig. S3C), but confirmed that acetylated
268 tubulin is enriched in the polar region of the spindle but absent from the central spindle
269 when the spindle elongates in anaphase (Fig. 4D).

270 Finally, poly-glutamylation, which is the addition of glutamate side chains of variable
271 length to the carboxy-terminal tail of both α- and ß-tubulin (Bodakuntla et al., 2021; Eddé
272 et al., 1990; RadiBer et al., 1992), is thought to modulate the interaction between
273 microtubules and their partners, MAPs (Microtubule Associated Proteins) and molecular
274 motors, affecting cargo movement, microtubule stability and severing (Bodakuntla et al.,
275 2021). Using the antibody GT335 against glutamylated tubulin (Wolff et al., 1992) we

276 showed that in *O.* cf. *ovata* glutamylated-tubulin is undetectable in non-dividing cells (Fig.
277 S3E, interphase). We could observe tubulin glutamylation exclusively in mitotic cells,
278 starting from early mitosis. As for tyrosinated tubulin, glutamylated tubulin was enriched
279 in the central spindle (Fig. S3E). Differently from acetylated and tyrosinated tubulin,
280 glutamylated-tubulin is not present at the site of cytokinesis.

281

282 **Centrin accumulates exclusively at basal bodies**

283 In eukaryotic cells centrioles and basal bodies are essential for the organization of the
284 microtubule cytoskeleton during interphase and mitosis (Wu and Akhmanova, 2017). A
285 well conserved component of both these structures is centrin, a calmodulin-like Ca^{2+}-
286 binding protein present in protists, yeast and animal cells. In the green algae *C. reinhardtii*,
287 where it was first identified, centrin localizes to the region of the basal body associated
288 with the flagellum axoneme during interphase, and re-localizes to spindle poles during
289 mitosis to organize the mitotic spindle (Salisbury et al., 1988). As genomic data are not
290 available for *O.* cf. *ovata* we generated transcriptomic data from cultured *O.* cf. *ovata* cells
291 (strain MCCV54) during exponential growth and searched for centrin homologues.
292 Analysis of this transcriptomic dataset allowed the identification of a centrin transcript in
293 *O.* cf. *ovata* with 55% identity to human centrin and 53% to *C. reinhardtii* centrin (Fig.
294 5A). Using a polyclonal antibody against *C. reinhardtii* centrin (20H5), we then sought to
295 identify microtubule organizing centres (MTOCs) in *O.* cf. *ovata* cells. In western blot
296 assays the 20H5 antibody recognizes a single *O.* cf. *ovata* protein of the expected (20kDa)
297 molecular weight (Fig. 5B). In cells the 20H5 antibody intensely labelled a structure in the
298 ventral region of the cell, near the flagella insertion site where the basal bodies are located
299 (Fig. 5C). In line with our observation that flagella are maintained during the entire cell
300 cycle (Fig. S1), we observed that centrin, which is required for flagellar motility (Fenchel,
301 2001), was maintained in the ventral area throughout mitosis and cytokinesis. Consistently,
302 we did not observe accumulation of centrin at spindle poles at any stage of mitosis,
303 supporting earlier EM studies suggesting that dinoflagellate spindles are acentriolar. The

304 centrin antibody also stained fibrous structures which extend from the basal bodies towards
305 both the cell centre and the cell cortex (Fig. 5C).

306 Based on our observations we cannot determine when basal body duplication takes place.
307 However, as shown in Fig. 5C we observed that the two centrin-labelled basal bodies are
308 juxtaposed in interphase, separate in mitosis and then segregate to the two daughter cells
309 in cytokinesis. Quantification of the distance between the two peaks of fluorescent intensity
310 in centrin-labelled cells confirmed this observation (Fig. 5D), showing that the two basal
311 bodies separate when the spindle forms as the distance between the two peaks remains
312 constant in interphase (average ± SD: 1,4 ± 0,4µm) and pre-mitotic cells (1,4 ± 0,3µm) but
313 increases to 2,7 µm (± 0,5 µm) in mitotic cells containing a fully formed spindle. In
314 telophase the cytokinetic plate then forms between the two fully segregated basal bodies
315 (5,6 ± 1,7 µm), generating two daughter cells with their own flagellar apparatus.

316

317 **Discussion**

318 Due to the unique characteristics of mitosis in dinoflagellates, the term dinomitosis has
319 been used to describe how chromosomes are segregated in those organisms. Here, we have
320 analysed cytoskeletal changes associated with dinomitosis and cytokinesis in the
321 dinoflagellate *O.* cf. *ovata*. which are summarized in Fig. 5 E. In interphase cells the
322 nucleus is located near the dorsal side of the cell and does not interact with microtubules
323 of the ventral bundle. Cortical microtubules run under the plasma membrane and as
324 previously shown for another dinoflagellate, *C. cohnii* (Perret et al., 1993), they persist
325 throughout the cell cycle, including mitosis and cytokinesis. This is similar to what was
326 observed in other unicellular organisms, such as *Trypanosoma brucei*, where the
327 subpellicular microtubule corset which is required for cell shape (Sinclair et al., 2021), is
328 maintained during cell division and is only remodelled locally at the site of furrow
329 formation during cytokinesis (Gull, 1999).

330 The first sign of preparation for mitosis in *O.* cf. *ovata* is the re-localization of the nucleus
331 to the centre of the cell. We observed that while in the cell centre, the nucleus is always

332 associated with microtubules of the ventral bundle and in few cells this association is also
333 observed while the nucleus is in dorsal position. This configuration suggests that nuclear
334 re-positioning is microtubule based and that extension and branching of the microtubule
335 bundle towards the dorsal side of the cell might be a pre-requisite for nucleus-microtubule
336 interaction and could be considered as an early indicator of preparation for mitosis. Centrin
337 filaments are also associated with the ventral bundle and with the basal bodies where the
338 ventral bundle originates from. It is therefore possible that nuclear movement relies not
339 only on the mechanical action of microtubules and associated motors but also on the
340 contractile activity of centrin, as already observed in nuclear repositioning during mitosis
341 in *C. reinhardtii* (Salisbury et al., 1988). In this organism the two flagella are reabsorbed
342 prior to division and during prophase two major microtubule fibres extend from the basal
343 bodies toward the nucleus and reposition it from the middle of the cell to the apical side,
344 where the basal bodies are located. Centrin which forms filamentous structures that link
345 the basal bodies to the nucleus (Geimer and Melkonian, 2005; Wright et al., 1989) provides
346 contractility to the microtubule bundles and contraction of centrin fibres at mitotic entry
347 allows nuclear movement towards the apical cell surface (Salisbury et al., 1988). This
348 movement is followed by separation of the basal bodies in prophase. Indeed, we observe a
349 similar separation of centrin-labelled bodies in early mitotic stages in *O.* cf. *ovata*.

350 Upon localization of the nucleus to the cell centre, the mitotic spindle forms, with 6-8
351 spindle microtubule bundles traversing the nucleus along the short axis of the cell, in line
352 with previous observations in other gonnyalucoid species, the dinoflagellate clade with the
353 highest number of nuclear tunnels (Gavelis et al., 2019). Throughout mitosis, the spindle
354 remains connected to the cell ventral cortex through two microtubule fibres that probably
355 originate from splitting of the ventral bundle. This configuration is similar to the three-
356 pronged fork described in *C. cohnii* where the spindle poles are connected to the basal
357 bodies by a bundle of microtubules, the desmoses (Perret et al., 1993). In animal, yeast and
358 several algal cells, spindle formation is usually driven by the centrosomes localized at
359 spindle poles. Although more markers will need to be analysed, the geometry of the spindle
360 with the association of spindle poles to the microtubules of the ventral bundle and the
361 absence of centrin accumulation at spindle poles suggests that *O.* cf. *ovata* spindles are

362 acentrosomal. Indeed, EM studies in other dinoflagellate species have never identified
363 centrioles in the vicinity of the nuclear membrane, with the only exception of Syndiniales
364 (Bhaud et al., 2000; Drechsler and McAinsh, 2012; Moon et al., 2015). Acentrosomal
365 spindle formation has been observed in animal and plant cells. In those cells spindle
366 organization is driven by chromosomes, often through the formation of a local gradient of
367 RanGTP (Deng et al., 2007; Lee and Liu, 2019). However, this is difficult to envisage for
368 dinomitosis as spindle microtubules are cytoplasmic and indirectly contact the
369 chromosomes which are connected to the inner side of the nuclear membrane.

370 Our analysis of microtubule PTMs allowed the identification of two regions in anaphase
371 spindles with different characteristics: a polar region highly acetylated and constant in
372 length (constant pole-DNA distance), which is anchored to the ventral area by the ventral
373 bundle, and a central spindle region which is instead enriched in tyrosinated tubulin and
374 whose length increases during mitosis (Fig. 4D,E). Similar to kinetochore microtubules in
375 animal spindles (Wilson and Forer, 1989), the stable acetylated microtubules link
376 chromosomes to spindle poles and most likely correspond to the k-fibers observed by EM
377 both in other dinoflagellates (Oakley and Dodge, 1976; Ris and Kubai, 1974) and in the
378 flagellate hypermastigote *Barbulanympha* (Inoué and Ritter, 1978; Ritter et al., 1978).
379 Different from most animal spindles, instead, the interpolar microtubules running between
380 opposite spindle poles, correspond to the tyrosinated microtubules described here.
381 Interestingly the tyrosinated microtubules never reach the spindle poles. In anaphase
382 spindles, tyrosinated microtubules appear to overlap with acetylated microtubules only in
383 the vicinity of the segregating chromosomes, possibly at the level of the kinetochores.
384 Based on these studies we suggest that during pro/metaphase of dinomitosis mitotic
385 chromosomes become anchored to opposite spindle poles by stable acetylated polar
386 microtubules. During anaphase polymerization of the more dynamic tyrosinated interpolar
387 microtubules then drives chromosome segregation (anaphase B) without prior poleward
388 chromosome movement towards the spindle poles, thus suggesting a lack of anaphase A.
389 The exact organization of the central microtubule array as well as the nature of the
390 molecular motors generating the pushing force remains unclear. Further studies will be
391 required to determine whether chromosome segregation relies on microtubule

392 polymerization or sliding of interdigitating central spindle microtubules. Either way, this
393 mechanism is reminiscent of the central-spindle driven chromosome segregation described
394 during meiosis in *C. elegans* oocytes (Laband et al., 2017) and during mitosis in *C. elegans*
395 embryos without centrosomes (Cowan and Hyman, 2004). In both cases, kinetochore
396 microtubules act as a scaffold to anchor chromosomes to spindle poles and correctly
397 localize them onto the metaphase plate during spindle polarization (Pitayu-Nugroho et al.,
398 2023), while polymerization of microtubules of the central spindle generates an outward
399 pushing force to allow chromosome segregation. The presence of this mechanism in
400 distantly related nematodes and dinoflagellates suggests that it might have emerged early
401 in evolution and could represent a primitive microtubule-based mechanism for
402 chromosome segregation which predates the evolution of cortical interactions to generate
403 pulling forces and ensure higher accuracy in chromosome segregation. Indeed, a similar
404 mechanism can also be observed in bacteria where segregation of low copy number
405 plasmids relies on the polymerization of antiparallel ParM filaments, whose elongation
406 pushes plasmid clusters towards the poles of the cell, allowing their segregation before cell
407 division (Gayathri et al., 2012).

408 Starting from anaphase, a microtubule-rich structure is formed from the dorsal side,
409 opposite the basal bodies. This structure coincides with the cleavage plane, suggesting a
410 direct implication for microtubules either in placement of the cleavage plane and/or
411 cytokinesis. This observation is in line with the idea that actomyosin driven cytokinesis is
412 a novel acquisition of unikont (animal, yeast and amoeba) cells. Indeed, the lack of Myosin
413 II in most bikont species (Richards and Cavalier-Smith, 2005), including dinoflagellates,
414 supports the use of alternative mechanisms for cytokinesis. In many unicellular protists and
415 in plant cells microtubules have a central role in cytokinesis and form specialized structures
416 associated with the site of cytokinesis. In plants phragmoplast microtubules form in the
417 centre of the cell and then expand centrifugally towards the cell membrane. In *C.*
418 *reinhardtii* and in other related green algae, instead, cytokinesis is associated with a special
419 array of microtubules, the phycoplast, which forms at the anterior end of the cell where the
420 microtubule rootlets are located and grows unidirectionally towards the opposite pole of
421 the cell (Ehler and Dutcher, 1998). The cytokinetic plate we described here for *Ostreopsis*

422 bears similarities with the algal phycoplast as it forms at the dorsal side and then grows in
423 a unidirectional fashion. However differently from *C. reinhardtii*, the cytokinetic plate
424 described here originates opposite to the basal bodies and grows towards them, suggesting
425 that, as already observed for the plant phragmoplast, the mechanism of microtubule
426 nucleation in the dinoflagellate cytokinetic plate is most likely independent of centrosomes
427 and basal bodies.

428

429 **Materials and Methods**

430 **Cell culture and bloom sampling**

431 Strains of O. cf. *ovata* (MCCV054) obtained from the Mediterranean Culture Collection of
432 Villefranche-sur-Mer (MCCV), EMBRC-France, were cultured in autoclaved and filtered
433 enriched seawater, at a salinity of 38 g/L, as described by Guillard and Hargraves (L1
434 enriched seawater medium) (Guillard and Hargraves, 1993). Cultures were incubated at 22
435 °C under a 14:10 light/dark cycle (250 µmol m-2 s-1). Cells were fixed for staining during
436 the proliferative phase (day 6 to 10) in order to obtain the greatest number of cells in
437 division.

438 Bloom samples were collected in Villefranche-sur-mer, on the Mediterranean French coast
439 (43°41′34.83″ N and 7°18′31.66″ E), where yearly blooms occur. Samples used for
440 immunofluorescence were collected in 2018, 2019 and 2020 between 12:00 pm and 4:00
441 am (Pavaux et al., 2021).

442 **Actin staining and immunofluorescence**

443 For immunofluorescence a previous published protocol was modified (Escalera et al.,
444 2014). Cells were fixed in cold fixative solution (80% methanol, 10% DMSO (Sigma-
445 Aldrich) and 0,5 mM EGTA pH 7.5 (from 0,5 M EGTA pH 7.5 stock solution in distilled
446 water)) for at least 24 hours, at -20ºC to improve membrane permeabilization. Samples
447 could be maintained in fixative solution for several months. When needed, samples were
448 rehydrated progressively in methanol-PBS (60%, 40%, 20%) and finally in PBS, with a 10
449 minutes incubation at each step. Cells were then permeabilized by two consecutive

450 incubations in PBT (PBS with 0.1% Triton X-100) for 15 minutes at room temperature
451 (RT). Cells were recovered by centrifugation, 5 minutes at 0.2 RCF, and then blocked for
452 30 minutes at RT in PBT containing 5% BSA (PBT-BSA) and then incubated at 4ºC in
453 PBT-BSA containing primary antibody at the appropriate dilution for 3-6 days to maximize
454 antibody penetration. With incubations shorter that 2 days structures deep into the
455 cytoplasm were not labelled. For microtubule staining, D66 anti β-tubulin antibody
456 (against tubulin from *Lytechinus pictus*, mouse, Sigma-Aldrich) was used at 1:400 dilution;
457 for acetylated tubulin, T6793 antibody (Clone 6- 11B-1, mouse, Sigma-Aldrich) was used
458 at 1:400 dilution; for tyrosinated tubulin, YL1/2 antibody (ab6160; rat, Abcam) was used
459 at 1:400 dilution; for polyglutamylated tubulin, monoclonal antibody anti
460 polyglutamylated (clone GT335, mouse, Adipogen); the anti-centrin antibody (clone
461 20H5; mouse, Merk) was used at 1:100 dilution.

462 After incubation with the primary antibody, cells were washed three times in PBT, and
463 then incubated over-night at 4ºC in PBT-BSA with the appropriate secondary antibody at
464 a 1:400 dilution (fluorescently-conjugated anti-mouse and anti-rat antibodies, Jackson
465 ImmunoResearch). After over-night incubation, cells were washed twice with PBS, and
466 then incubated for 10 minutes with 1μg/ml Hoechst-33342 (Sigma-Aldrich) to label the
467 DNA, rinsed twice with PBS and finally resuspended in 100-200 μl of PBS. 50 μl of cells
468 were mixed with 50 μl of citiflour AF1 (Science Services) and mounted on slides for
469 imaging. Each experiment was repeated 3-5 times, 25-50 cells were counted for each
470 sample and 5-15 images were collected for further analysis.

471 Actin filaments were visualized using CytoPainter Phalloidin-iFluor 488 Reagent
472 (ab176753, Abcam). Cells were fixed in 4% paraformaldehyde in PBS for at least 24 hours
473 at 4ºC. Cells were then washed three times in PBS and permeabilized as described for
474 immunofluorescence. After a 30-minute incubation in PBT-BSA, cells were then incubated
475 in PBT containing phalloidin at 1:400 dilution, for 1 hour at RT in the dark. Cells were
476 then washed twice in PBS, and mounted in citiflour AF1 (Science Services) for immediate
477 imaging.

478 Images were acquired with Leica SP8 and Stellaris 5 microscopes both equipped with a
479 63X/1.4 Oil and a 40X/1.1W objective, which are part of the Plateforme d'Imagerie
480 Microscopique (PIM) of the Institute de la mer de Villefranche sur mer. On stellaris 5
481 images were deconvolved with Lightning. When present, Z-Drift was corrected using a
482 custom-made tool (https://github.com/SebastienSchaub/SatAndDriftEstimator). Spindle
483 measurements and image analysis were performed in Fiji (49) with home-made 3D
484 distance tool (https://github.com/SebastienSchaub/3DtDist) and visualization on Imaris
485 (Imaris, BitPlane, Zurich, Switzerland).

486 **Protein extraction and western blot analysis**

487 To test antibodies, proteins were extracted from cells of strain MCCV-054. 50 ml of cells
488 were grown in L1 media and collected 14 days after inoculum by filtration through
489 Durapore 5 µm PDVF membranes (Millipore) using a manifold system. Cells were
490 recovered from the filters in 1 ml of PBS and then pelleted by centrifugation at 5000rpm
491 for 5 minutes. Pellets were then fast frozen in liquid nitrogen, then resuspended in an equal
492 volume of 2x Laemmli (100 mM Tris-HCl at pH 6.8, 4% SDS, 0.2% bromophenol blue,
493 20% glycerol, 200 mM dithiothreitol) and heated at 100ºC for 5 minutes. Samples were
494 separated on a 10% SDS-polyacrylamide gel and then transferred to a nitrocellulose
495 membrane. Membranes were blocked for 1h in Tris Buffer-Saline (TBS: 20 mM Tris Base,
496 150 mM NaCl) containing 2% milk, 0.1% tween-20 (TBS-Tween-milk) and then incubated
497 in blocking solution containing the appropriate antibody overnight at 4°C. For centrin
498 detection the 20H5 antibody (Merck) was diluted 1:2000, for detection of tubulin (DM1a
499 antibody, Sigma-Aldrich, mouse) and of PTMs (tyrosinated tubulin: YL ½ antibody,
500 ab6160; rat monoclonal, Abcam; acetylated tubulin: T6793 antibody, clone 6-11B-1,
501 mouse, Sigma-Aldrich; polyglutamylated tubulin: GT335, mouse, Adipogen) all
502 antibodies were diluted 1:3000. Following antibody incubation, membranes were washed
503 3 times with TBS-Tween (TBS with 0.1% tween-20) and incubated with an appropriate
504 horseradish peroxidase-conjugated secondary antibody (Jackson ImmunoResearch) at
505 1:10000 dilution in TBS-Tween-milk for 1 hour at RT. After 3 washes with TBS-Tween,
506 signal detection was carried out using the SuperSignal West Pico chemio-luminescent

507 substrate (Thermo Scientific) as described by the manufacturer and imaged in the Vilmen-
508 Loubet Fusion machine.
509
510 **RNA extraction, transcriptome annotation and sequence analysis**
511 For RNA sequencing total RNA was extracted from cells of strain MCCV-054. 150 ml of
512 cells were grown in L1 media and collected 6, 12 and 18 days after initial inoculum as for
513 protein preparation.

514 Filters with cells were placed in 1ml of TRI-reagent (Sigma-Aldrich) and incubated on ice
515 for five minutes. Cells were broken by beating in the presence of ~ 3 g of glass beads
516 (Sigma) in a 220 V bead beater at 4000 rpm for 40s. RNA was then extracted using a
517 RiboPureTM (Ambion) kit following the manufacturer's instructions. Residual DNA was
518 removed by treatment with DNase I (Q1 DNAse, Promega) for 1h at 37 °C (2 units per
519 sample) followed by purification with the RNeasy miniElute Cleanup kit (Qiagen).

520 RNA purity, quantity and integrity were assessed for each sample using a Nanodrop ND-
521 1000 and 2100 Bioanalyser. RNA samples were then sent to BGI-Tech, China for library
522 generation and sequencing with the DNBSEQ™ technology platforms to generate 100 base
523 pair (bp) paired end reads.

524 *De novo* assembly of reads was carried out with Trinity version 2.4.0 (Grabherr et al., 2011)
525 using default parameters. The full assembly was filtered to the longest transcript per gene
526 group making use of the '_i' designations of the Trinity transcript identifiers. Open reading
527 frames were predicted using TransDecoder v5.3. These protein sequences were searched
528 against the NCBI NR database and sequences whose best hit was to Dinophyceae were
529 retained. To annotate these sequences, the pantherScore2.1.pl script was used to search
530 them against the PANTHER hidden Markov model library (version 14.1). Multiple
531 sequence alignments were performed using Clustal Omega and viewed using Jalview Vs
532 2-a (Waterhouse et al., 2009).

533
534

Acknowledgments

We are grateful to L. Besnardeau for technical support, to E. Christians, S. Marro and M. Hagström for discussion and sharing of reagents, to J. Chenevert and R. Copley for critical reading of the manuscript. We thank the imaging platform, PIM (member of the MICA microscopy platform) where image acquisition was conducted. PIM is supported by EMBRC-France, whose French state funds are managed by the ANR within the investments for the future program under reference ANR-10-INSB-02. DV was supported by Minciencias- Colombia - financial support 783, PhD program.

Competing interests

No competing interests declared

References

Bhaud, Y., Guillebault, D., Lennon, J., Defacque, H., Soyer-Gobillard, M.O., Moreau, H., 2000. Morphology and behaviour of dinoflagellate chromosomes during the cell cycle and mitosis. J Cell Sci 113, 1231–1239.

Bodakuntla, S., Janke, C., Magiera, M.M., 2021. Tubulin polyglutamylation, a regulator of microtubule functions, can cause neurodegeneration. Neuroscience Letters 746, 135656. https://doi.org/10.1016/j.neulet.2021.135656

Bravo, I., Vila, M., Casabianca, S., Rodriguez, F., Rial, P., Riobó, P., Penna, A., 2012. Life cycle stages of the benthic palytoxin-producing dinoflagellate *Ostreopsis* cf. *ovata* (Dinophyceae). Harmful Algae 18, 24–34. https://doi.org/10.1016/j.hal.2012.04.001

Bulinski, J.C., Richards, J.E., Piperno, G., 1988. Posttranslational modifications of alpha tubulin: detyrosination and acetylation differentiate populations of interphase microtubules in cultured cells. Journal of Cell Biology 106, 1213–1220. https://doi.org/10.1083/jcb.106.4.1213

Cachon, J., Cachon, M., 1977. Observations on the mitosis and on the chromosome evolution during the lifecycle of *Oodinium*, a parasitic dinoflagellate. Chromosoma 60, 237–251. https://doi.org/10.1007/BF00329773

Cowan, C.R., Hyman, A.A., 2004. Centrosomes direct cell polarity independently of microtubule assembly in *C. elegans* embryos. Nature 431, 92–96. https://doi.org/10.1038/nature02825

568 Cross, F.R., Umen, J.G., 2015. The Chlamydomonas cell cycle. Plant J 82, 370–392.
569 https://doi.org/10.1111/tpj.12795
570 Deng, M., Suraneni, P., Schultz, R.M., Li, R., 2007. The Ran GTPase Mediates
571 Chromatin Signaling to Control Cortical Polarity during Polar Body Extrusion in
572 Mouse Oocytes. Developmental Cell 12, 301–308.
573 https://doi.org/10.1016/j.devcel.2006.11.008
574 Drechsler, H., McAinsh, A.D., 2012. Exotic mitotic mechanisms. Open Biol 2.
575 https://doi.org/10.1098/rsob.120140
576 Driscoll, W.W., Hackett, J.D., Ferrière, R., 2016. Eco-evolutionary feedbacks between
577 private and public goods: evidence from toxic algal blooms. Ecol Lett 19, 81–97.
578 https://doi.org/10.1111/ele.12533
579 Eddé, B., Rossier, J., Le Caer, J.-P., Desbruyères, E., Gros, F., Denoulet, P., 1990.
580 Posttranslational Glutamylation of α-tubulin. Science 247, 83–85.
581 https://doi.org/10.1126/science.1967194
582 Ehler, L.L., Dutcher, S.K., 1998. Pharmacological and genetic evidence for a role of
583 rootlet and phycoplast microtubules in the positioning and assembly of cleavage
584 furrows in *Chlamydomonas reinhardtii.* Cell Motil Cytoskeleton 40, 193–207.
585 https://doi.org/10.1002/(SICI)1097-0169(1998)40:2<193::AID-CM8>3.0.CO;2-G
586 Escalera, L., Benvenuto, G., Scalco, E., Zingone, A., Montresor, M., 2014.
587 Ultrastructural Features of the Benthic Dinoflagellate *Ostreopsis* cf. *ovata*
588 (Dinophyceae). Protist 165, 260–274. https://doi.org/10.1016/j.protis.2014.03.001
589 Eshun-Wilson, L., Zhang, R., Portran, D., Nachury, M.V., Toso, D.B., Löhr, T.,
590 Vendruscolo, M., Bonomi, M., Fraser, J.S., Nogales, E., 2019. Effects of α-
591 tubulin acetylation on microtubule structure and stability. Proc Natl Acad Sci
592 USA 116, 10366–10371. https://doi.org/10.1073/pnas.1900441116
593 Fenchel, T., 2001. How Dinoflagellates Swim. Protist 152, 329–338.
594 https://doi.org/10.1078/1434-4610-00071
595 Francia, M.E., Dubremetz, J.-F., Morrissette, N.S., 2015. Basal body structure and
596 composition in the apicomplexans Toxoplasma and Plasmodium. Cilia 5, 3.
597 https://doi.org/10.1186/s13630-016-0025-5
598 Gavelis, G.S., Herranz, M., Wakeman, K.C., Ripken, C., Mitarai, S., Gile, G.H., Keeling,
599 P.J., Leander, B.S., 2019. Dinoflagellate nucleus contains an extensive
600 endomembrane network, the nuclear net. Scientific Reports 9.
601 https://doi.org/10.1038/s41598-018-37065-w
602 Gayathri, P., Fujii, T., Møller-Jensen, J., Van Den Ent, F., Namba, K., Löwe, J., 2012. A
603 Bipolar Spindle of Antiparallel ParM Filaments Drives Bacterial Plasmid
604 Segregation. Science 338, 1334–1337. https://doi.org/10.1126/science.1229091
605 Geimer, S., Melkonian, M., 2005. Centrin Scaffold in *Chlamydomonas reinhardtii*
606 Revealed by Immunoelectron Microscopy. Eukaryot Cell 4, 1253–1263.
607 https://doi.org/10.1128/EC.4.7.1253-1263.2005
608 Grabherr, M.G., Haas, B.J., Yassour, M., Levin, J.Z., Thompson, D.A., Amit, I.,
609 Adiconis, X., Fan, L., Raychowdhury, R., Zeng, Q., Chen, Z., Mauceli, E.,
610 Hacohen, N., Gnirke, A., Rhind, N., di Palma, F., Birren, B.W., Nusbaum, C.,
611 Lindblad-Toh, K., Friedman, N., Regev, A., 2011. Full-length transcriptome

assembly from RNA-Seq data without a reference genome. Nat Biotechnol 29, 644–652. https://doi.org/10.1038/nbt.1883

Guillard, R.R.L., Hargraves, P.E., 1993. S*tichochrysis immobilis* is a diatom, not a chrysophyte. Phycologia 32, 234–236. https://doi.org/10.2216/i0031-8884-32-3-234.1

Gull, K., 1999. The Cytoskeleton of Trypanosomatid Parasites. Annu. Rev. Microbiol. 53, 629–655. https://doi.org/10.1146/annurev.micro.53.1.629

Hammarton, T.C., 2019. Who Needs a Contractile Actomyosin Ring? The Plethora of Alternative Ways to Divide a Protozoan Parasite. Front. Cell. Infect. Microbiol. 9, 397. https://doi.org/10.3389/fcimb.2019.00397

Inoué, S., Ritter, H., 1978. Mitosis in *Barbulanympha.* II. Dynamics of a two-stage anaphase, nuclear morphogenesis, and cytokinesis. The Journal of cell biology 77, 655–684. https://doi.org/10.1083/jcb.77.3.655

Janke, C., 2013. Mysterious modification of tubulin. Nat Rev Mol Cell Biol 14, 692–692. https://doi.org/10.1038/nrm3685

Kilmartin, J.V., Wright, B., Milstein, C., 1982. Rat monoclonal antitubulin antibodies derived by using a new nonsecreting rat cell line. The Journal of cell biology 93, 576–582. https://doi.org/10.1083/jcb.93.3.576

Laband, K., Le Borgne, R., Edwards, F., Stefanutti, M., Canman, J.C., Verbavatz, J.-M., Dumont, J., 2017. Chromosome segregation occurs by microtubule pushing in oocytes. Nat Commun 8, 1499. https://doi.org/10.1038/s41467-017-01539-8

Lee, Y.J., Liu, B., 2019. Microtubule nucleation for the assembly of acentrosomal microtubule arrays in plant cells. New Phytol 222, 1705–1718. https://doi.org/10.1111/nph.15705

Moon, E., Nam, S.W., Shin, W., Park, M.G., Coats, D.W., 2015. Do All Dinoflagellates have an Extranuclear Spindle? Protist 166, 569–584. https://doi.org/10.1016/j.protis.2015.08.005

Ninčević Gladan, Ž., Arapov, J., Casabianca, S., Penna, A., Honsell, G., Brovedani, V., Pelin, M., Tartaglione, L., Sosa, S., Dell'Aversano, C., Tubaro, A., Žuljević, A., Grbec, B., Čavar, M., Bužančić, M., Bakrač, A., Skejić, S., 2019. Massive Occurrence of the Harmful Benthic Dinoflagellate *Ostreopsis* cf. *ovata* in the Eastern Adriatic Sea. Toxins 11, 300. https://doi.org/10.3390/toxins11050300

Nishihama, R., Machida, Y., 2001. Expansion of the phragmoplast during plant cytokinesis: a MAPK pathway may MAP it out. Current Opinion in Plant Biology 4, 507–512. https://doi.org/10.1016/S1369-5266(00)00208-9

Oakley, B.R., Dodge, J.D., 1976. Mitosis and cytokinesis in the dinoflagellate *Amphidinium carterae*. Cytobios 17, 35–46.

Oakley, B.R., Dodge, J.D., 1974. Kinetochores associated with the nuclear envelope in the mitosis of a dinoflagellate. J Cell Biol 63, 322–325.

Onishi, M., Umen, J.G., Cross, F.R., Pringle, J.R., 2020. Cleavage-furrow formation without F-actin in *Chlamydomonas*. Proc Natl Acad Sci USA 117, 18511–18520. https://doi.org/10.1073/pnas.1920337117

Parsons, M.L., Aligizaki, K., Bottein, M.-Y.D., Fraga, S., Morton, S.L., Penna, A., Rhodes, L., 2012. *Gambierdiscus* and *Ostreopsis*: Reassessment of the state of

knowledge of their taxonomy, geography, ecophysiology, and toxicology. Harmful Algae 14, 107–129. https://doi.org/10.1016/j.hal.2011.10.017

Pavaux, A.-S., Velasquez-Carjaval, D., Drouet, K., Lebrun, A., Hiroux, A., Marro, S., Christians, E., Castagnetti, S., Lemée, R., 2021. Daily variations of *Ostreopsis* cf. *ovata* abundances in NW Mediterranean Sea. Harmful Algae 110, 102144. https://doi.org/10.1016/j.hal.2021.102144

Perret, E., Davoust, J., Albert, M., Besseau, L., Soyer-Gobillard, M.O., 1993. Microtubule organization during the cell cycle of the primitive eukaryote dinoflagellate *Crypthecodinium cohnii*. J Cell Sci 104 (Pt 3), 639–651.

Pitayu-Nugroho, L., Aubry, M., Laband, K., Geoffroy, H., Ganeswaran, T., Primadhanty, A., Canman, J.C., Dumont, J., 2023. Kinetochore component function in *C. elegans* oocytes revealed by 4D tracking of holocentric chromosomes. Nat Commun 14, 4032. https://doi.org/10.1038/s41467-023-39702-z

RadiBer, M., Plessman, U., KlOppelh, K.-D., 1992. Class II tubulin, the major brain,6 tubulin isotype is polyglutamylated on glutamic acid residue 435. FEBS LETTERS.

Rhodes, L., 2011. World-wide occurrence of the toxic dinoflagellate genus *Ostreopsis Schmidt*. Toxicon 57, 400–407. https://doi.org/10.1016/j.toxicon.2010.05.010

Richards, T.A., Cavalier-Smith, T., 2005. Myosin domain evolution and the primary divergence of eukaryotes. Nature 436, 1113–1118. https://doi.org/10.1038/nature03949

Ris, H., Kubai, D.F., 1974. An unusual mitotic mechanism in the parasitic protozoan *Syndinium* sp. Journal of Cell Biology 60, 702–720. https://doi.org/10.1083/jcb.60.3.702

Ritter, H., Inoué, S., Kubai, D., 1978. Mitosis in *Barbulanympha*. I. Spindle structure, formation, and kinetochore engagement. The Journal of cell biology 77, 638–654. https://doi.org/10.1083/jcb.77.3.638

Rosenbaum, J.L., Moulder, J.E., Ringo, D.L., 1969. Flagellar elongation and shortening in Chlamydomonas. Journal of Cell Biology 41, 600–619. https://doi.org/10.1083/jcb.41.2.600

Salisbury, J.L., Baron, A.T., Sanders, M.A., 1988. The centrin-based cytoskeleton of *Chlamydomonas reinhardtii*: distribution in interphase and mitotic cells. Journal of Cell Biology 107, 635–641. https://doi.org/10.1083/jcb.107.2.635

Schnepf, E., 1988. Cytochalasin D inhibits completion of cytokinesis and affects theca formation in dinoflagellates. Protoplasma 143, 22–28. https://doi.org/10.1007/BF01282955

Schnepf, E., Winter, S., Storck, I., Quader, H., 1990. A complementary experimental study of cell division in the dinoflagellate *Prorocentrum micans*. European Journal of Protistology 25, 234–242. https://doi.org/10.1016/S0932-4739(11)80175-6

Schulze, E., Asai, D.J., Bulinski, J.C., Kirschner, M., 1987. Posttranslational modification and microtubule stability. Journal of Cell Biology 105, 2167–2177. https://doi.org/10.1083/jcb.105.5.2167

Sherwin, T., Gull, K., Vickerman, K., 1989. The cell division cycle of T*rypanosoma brucei*: timing of event markers and cytoskeletal modulations. Philosophical

Transactions of the Royal Society of London. B, Biological Sciences 323, 573–588. https://doi.org/10.1098/rstb.1989.0037

Sinclair, A.N., Huynh, C.T., Sladewski, T.E., Zuromski, J.L., Ruiz, A.E., de Graffenried, C.L., 2021. The *Trypanosoma brucei* subpellicular microtubule array is organized into functionally discrete subdomains defined by microtubule associated proteins. PLoS Pathog 17, e1009588. https://doi.org/10.1371/journal.ppat.1009588

Stires, J.C., Latz, M.I., 2018. Contribution of the cytoskeleton to mechanosensitivity reported by dinoflagellate bioluminescence. Cytoskeleton 75, 12–21. https://doi.org/10.1002/cm.21392

Villanueva, M.A., Arzápalo-Castañeda, G., Castillo-Medina, R.E., 2014. The actin cytoskeleton organization and disorganization properties of the photosynthetic dinoflagellate *Symbiodinium kawagutii* in culture. Can. J. Microbiol. 60, 767–775. https://doi.org/10.1139/cjm-2014-0325

Waterhouse, A.M., Procter, J.B., Martin, D.M.A., Clamp, M., Barton, G.J., 2009. Jalview Version 2—a multiple sequence alignment editor and analysis workbench. Bioinformatics 25, 1189–1191. https://doi.org/10.1093/bioinformatics/btp033

Wetherbee, R., 1975. The fine structure of *Ceratium tripos*, a marine armored dinoflagellate. Journal of Ultrastructure Research 50, 77–88. https://doi.org/10.1016/S0022-5320(75)90010-6

Wilson, P.J., Forer, A., 1989. Acetylated a-tubulin in spermatogenic cells of the crane fly *Nephrotoma suturalis*: Kinetochore microtubules are selectively acetylated. Cell Motil. Cytoskeleton 14, 237–250. https://doi.org/10.1002/cm.970140210

Wolff, A., de Néchaud, B., Chillet, D., Mazarguil, H., Desbruyères, E., Audebert, S., Eddé, B., Gros, F., Denoulet, P., 1992. Distribution of glutamylated alpha and beta-tubulin in mouse tissues using a specific monoclonal antibody, GT335. Eur J Cell Biol 59, 425–432.

Wright, R.L., Adler, S.A., Spanier, J.G., Jarvik, J.W., 1989. Nucleus-basal body connector in Chlamydomonas: Evidence for a role in basal body segregation and against essential roles in mitosis or in determining cell polarity. Cell Motil. Cytoskeleton 14, 516–526. https://doi.org/10.1002/cm.970140409

Wu, J., Akhmanova, A., 2017. Microtubule-Organizing Centers. Annu. Rev. Cell Dev. Biol. 33, 51–75. https://doi.org/10.1146/annurev-cellbio-100616-060615

Figures

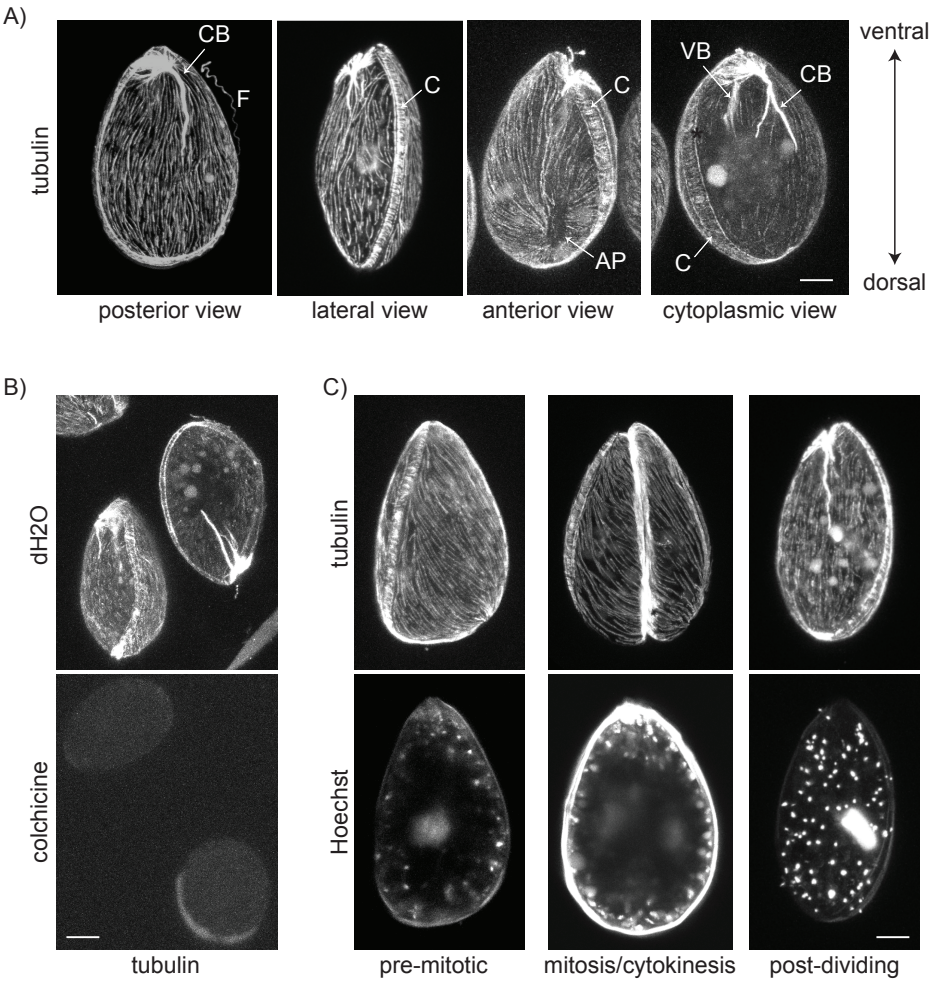

Figure 1. The cortical microtubule array is maintained during mitosis and cytokinesis.

(A) Representative confocal images of *O.* cf. *ovata* cells stained for ß-tubulin (D66 anti-ß-tubulin antibody). F= flagellum, AP= apical pore; VB= ventral bundle; CB= cortical bundle; C= cingulum. **(B)** Representative confocal images of control (dH2O) and colchicine (2µM) treated *O.* cf. *ovata* cells stained for ß-tubulin (D66 antibody). **(C)** Representative confocal images of pre-mitotic, mitotic and post-dividing *O.* cf. *ovata* cells stained for ß-tubulin (top, D66 antibody) and with Hoechst (DNA, bottom). Hoechst also stains DNA in mitochondria and chloroplasts. All cells are oriented with the ventral side on top, with the only exception of dH2O treated cells in B. All images are projections of the confocal Z-stack covering the whole cell. Scale bars are 10µm.

745

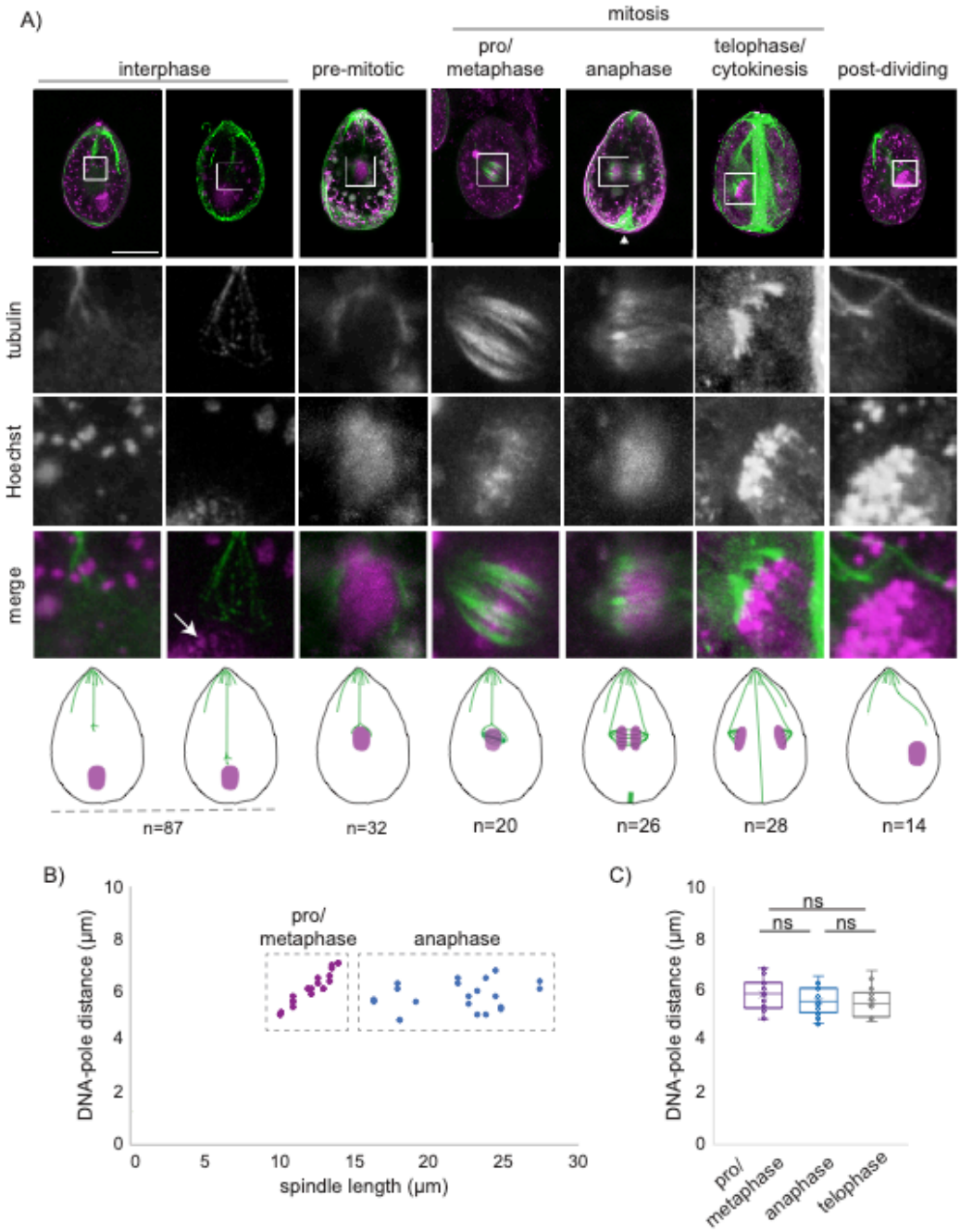

Figure 2: Changes in microtubule organization during dinomitosis.

746

747 **Figure 2. Changes in microtubule organization during dinomitosis.**

748 **(A)** Representative confocal images of *O.* cf. *ovata* cells at different cell cycle stages
749 stained with Hoechst (DNA, magenta) and for tubulin (green) using the D66 anti-ß-tubulin
750 antibody. White squares indicate the cell region enlarged underneath each image. All cells
751 are oriented with the ventral side on top. All images are projections of the confocal Z-stack
752 covering the nucleus. Schematic representations of microtubules and nucleus at each
753 analysed cell cycle stage are reported at the bottom. Arrow points to DNA; arrowhead to
754 forming cytokinetic structure. Number of analysed cells (n) is given for each stage. (**B)**
755 DNA-to-spindle pole distance as a function of total spindle length (pole to pole) in
756 pro/metaphase (red) and anaphase (blue) cells. Each dot corresponds to half a spindle. (**C)**
757 Quantification of DNA-to-spindle pole distance in cells at different mitotic stages. Each
758 dot represents half a spindle. Boxes represent 25-75th percentiles, and the mean is shown.
759 T-test was performed using all data points and retrieved non-significant difference (ns).
760 Scale bars are 20 µm.

761

762

763

764

765

766

767

768

769

770

771

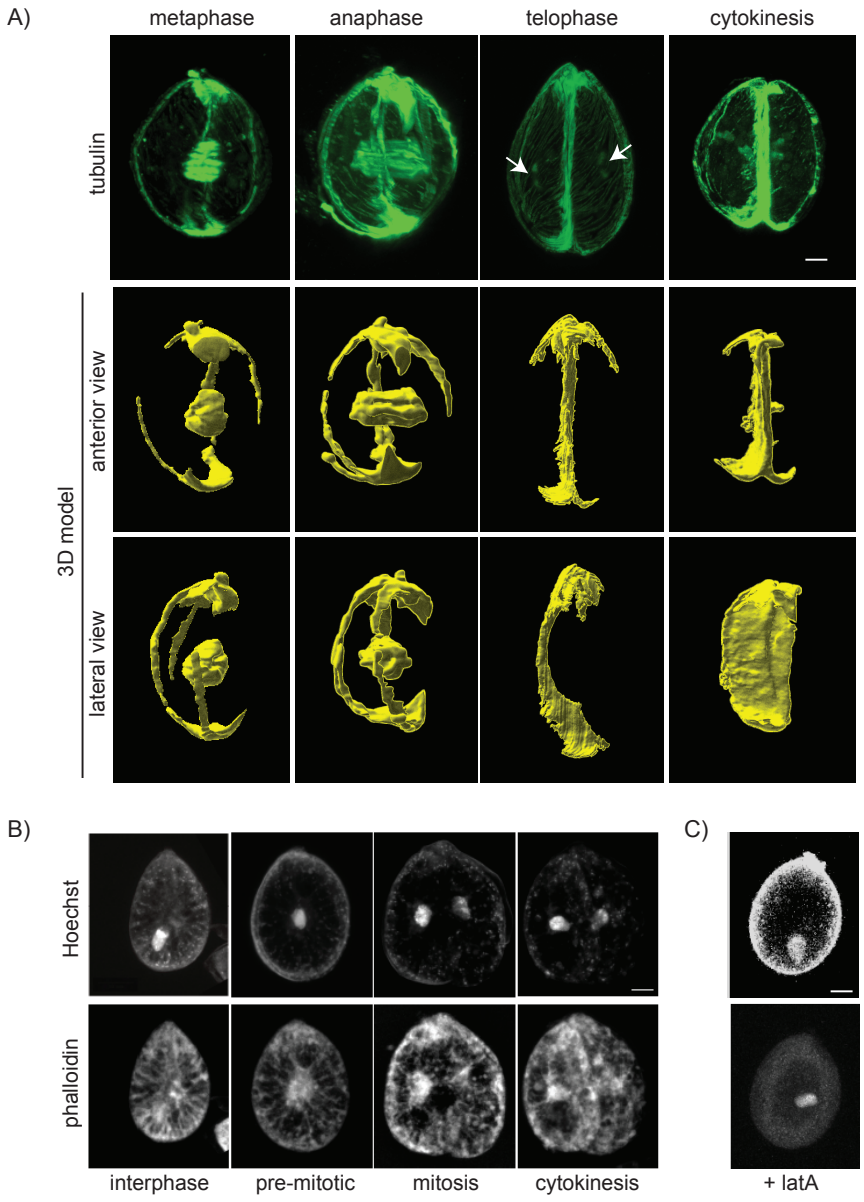

Figure 3. A microtubule-rich plate divides daughter cells in cytokinesis.
(A) Confocal images (top) and corresponding 3-D reconstructions (anterior view, middle; lateral view: rotation of anterior view by 90 degrees to the right, bottom) of mitotic cells stained for tubulin using the D66 anti-ß-tubulin antibody. Arrows point to telophase polar spindle. (B) Representative confocal images of *O.* cf. *ovata* cells at different cell cycle stages or (C) of cells treated with the actin depolymerizing drug latranculin A, stained with Hoechst (DNA, top) and with phalloidin (actin, bottom).
All cells are oriented with the ventral side on top. Scale bars are 10 µm.

772

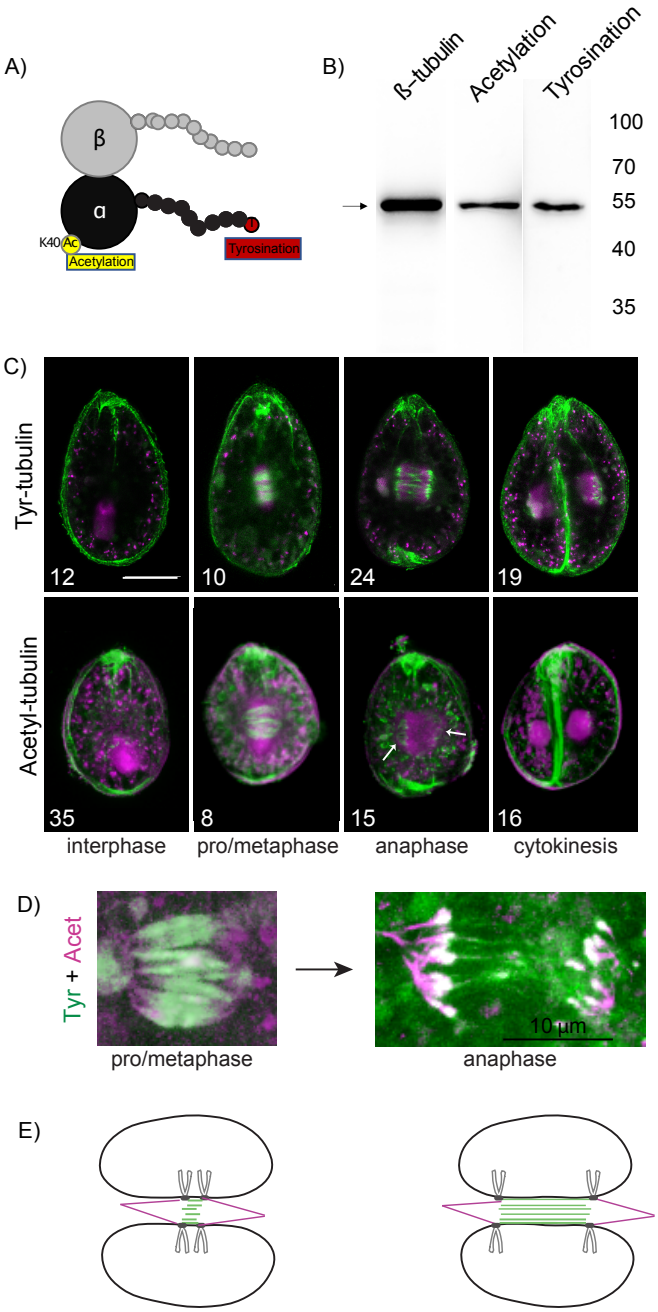

Figure 4: Tubulin post-translational modifications identify different microtubule populations

773

774 **Figure 4. Tubulin post-translational modifications identify different microtubule**
775 **populations**

776 **(A)** Schematic representation of a α- (black) and β– (grey) tubulin dimer with some
777 posttranslational modifications. **(B)** Western blot analysis of ß-tubulin and tubulin post-
778 translational modifications in whole protein extract from *O.* cf. *ovata* cells. **(C)**
779 Representative confocal images of *O.* cf. *ovata* cells stained with Hoechst (DNA, magenta),
780 and for tubulin with various PTMs (green): tyrosinated tubulin (YL1/2 antibody, top), or
781 acetylated tubulin (T6793 antibody, bottom). The number of analysed cells is indicated on
782 each image. **(D)** Confocal image of *O.* cf. *ovata* pro/metaphase (left) and anaphase (right)
783 spindles co-stained for tyrosinated tubulin (YL1/2 antibody, green), or acetylated tubulin
784 (T6793 antibody, magenta). **(E)** Schematic representation of mitotic nuclei with metaphase
785 and anaphase spindles: chromosomes are in light grey, kinetochore like structures in dark
786 grey, nuclear membrane in black, tyrosinated tubulin in green and acetylated tubulin in
787 magenta. Only 4 chromosomes are represented for simplicity. Scale bars are 20 µm, unless
788 otherwise stated.

789

790

791

792

793

794

795

796

797

798

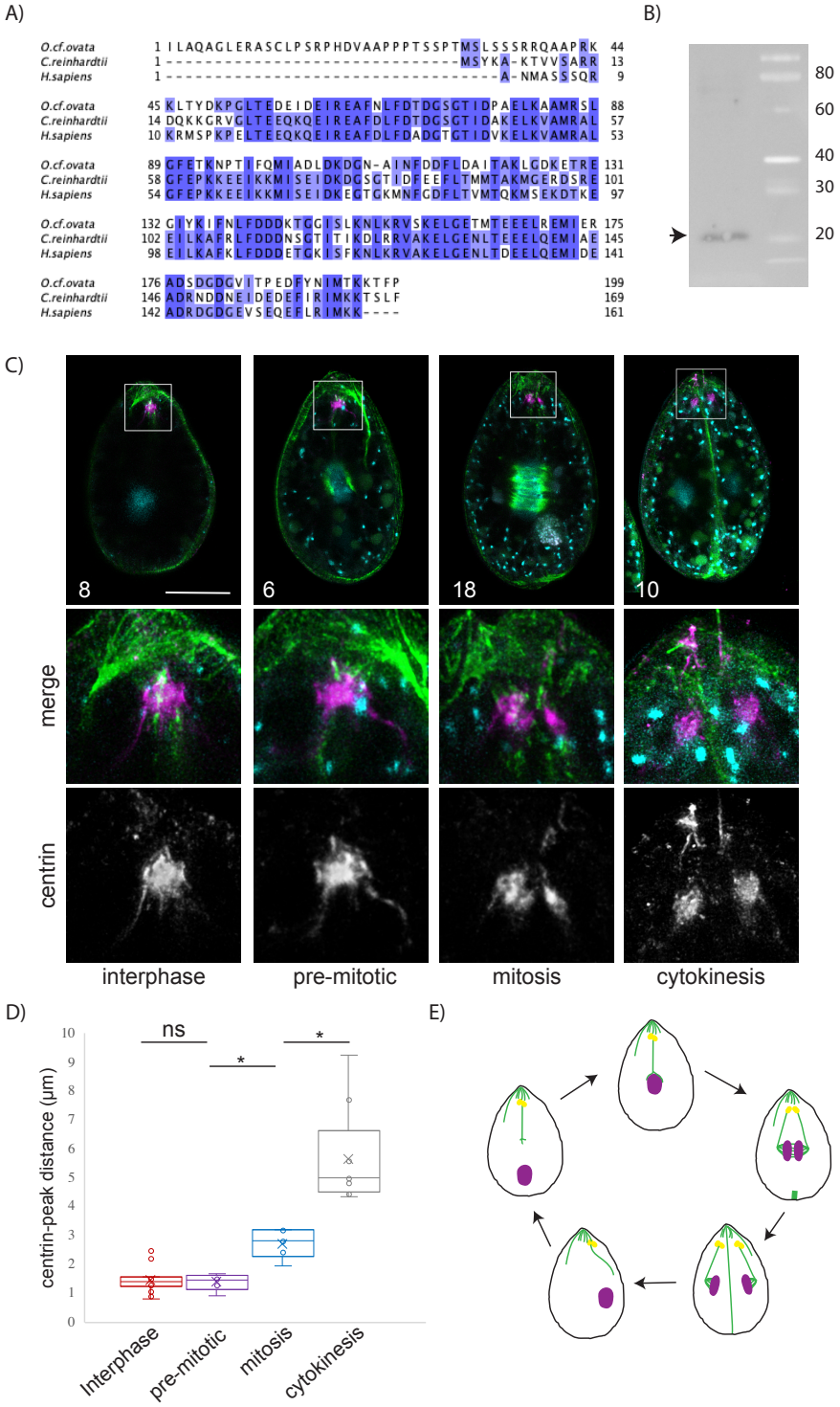

Figure 5: Centrin localizes to basal bodies throughout the mitotic cycle.

799

800 **Figure 5. Centrin localizes to basal bodies throughout the mitotic cycle.**

801 **(A)** Alignment of centrin sequences from *O.* cf. *ovata, C. reinhardtii***,** and *Homo sapiens*.
802 Coloured residues (blue) are identical across species. **(B)** Western blot analysis of centrin
803 in whole protein extract from *O.* cf. *ovata* cells. **(C)** Representative confocal images of *O.*
804 cf. *ovata* cells stained with Hoechst (DNA, cyan), for tubulin using the YL1/2 rat anti-□-
805 tubulin antibody (green) and for centrin using the mouse 20HA antibody against centrin
806 (magenta). White squares indicate the cell region enlarged underneath each image. All cells
807 are oriented with the ventral side on top. All images are projections of the confocal Z-stack
808 covering the nucleus. **(D**) Quantification of distance between peaks of fluorescence
809 corresponding to centrin staining at different cell cycle stages. T-test was performed using
810 all data points and retrieved either non-significant difference (ns) or a p value < 0,001 (*).
811 **(E)** Schematic representation of changes in nuclear and basal body position and
812 microtubule organization during the mitotic cell division cycle of *O.* cf. *ovata*. Scale bars
813 are 20 µm.
814